Open Access Research Journal of
Biology and Pharmacy
Journals home page: https://oarjbp.com/
ISSN: 2782-9979 (Online)

(REVIEW ARTICLE)

Assessment of FDA-Approved Antiviral Drugs Indicated for Different Viral Infections Against Crimean-Congo Hemorrhagic Fever Virus: Molecular Docking and Molecular Dynamics Simulations

Hamzah Mahmood Najm [1], Ahamed Mahdi Hassan [2,*] and Nermen R. Ahmed [3]

[1] *Kirkuk Health Directorate, Kirkuk, Iraq.*
[2] *Department of Biology, College of Sciences, University of Kirkuk, Kirkuk, Iraq.*
[3] *Department of Chemistry, College of Sciences, University of Kirkuk, Kirkuk, Iraq.*

Open Access Research Journal of Biology and Pharmacy, 2026, 16(02), 001-015

Publication history: Received on 16 January 2026; revised on 05 March 2026; accepted on 07 March 2026

Article DOI: https://doi.org/10.53022/oarjbp.2026.16.2.0021

Abstract

Background: Crimean-Congo hemorrhagic fever (CCHF) is a life-threatening viral disease characterized by high mortality rates and an increasing prevalence in endemic regions. Currently, no FDA-approved therapeutics are available for Crimean-Congo hemorrhagic fever virus (CCHFV) infection, and Ribavirin remains the only empirically used treatment option.

Method: In this study, we investigate the antiviral potential of six broad-spectrum agents Darunavir, Favipiravir, Nelfinavir, Remdesivir, Ritonavir, and Sofosbuvir against CCHFV using a structure-based drug design approach. Consensus molecular docking (MD), binding free energy calculations (MM-GBSA), and 100-nanosecond molecular dynamics simulations (MDS) were employed to evaluate the binding stability and affinity of these compounds to the viral target.

Results: Several agents, particularly Remdesivir, exhibited strong and stable interactions with the viral target, with binding energies comparable to or exceeding those of Ribavirin, indicating their potential efficacy.

Conclusion: Given their established antiviral activity against various RNA viruses, these agents merit further investigation as potential inhibitors of CCHFV replication, underscoring the promise of drug repurposing strategies for combating emerging viral threats.

Keywords: Crimean-Congo Hemorrhagic Fever; Antiviral Drug Repurposing; Molecular Docking; Molecular Dynamic Simulation; Remdesivir

1. Introduction

The Crimean-Congo hemorrhagic fever virus (CCHFV) is a globally distributed pathogen with high pathogenicity, causing severe hemorrhagic fever in humans and exhibiting a case fatality rate of up to 40% [1, 2]. The main vectors of the disease are ticks of the genus Hyalomma, along with the virus's widespread distribution across Europe. This phenomenon makes transmission of the virus through bites of infected *Hyalomma* ticks a more probable explanation [2]. In addition to tick bites, transmission can occur through contact with the blood or tissues of infected animals, and, in rare cases, human-to-human spread has been reported [3, 4]. Indeed, CCHFV is listed as a priority pathogen by WHO due to factors such as an expanding climatic range, the ability to infect migratory birds and livestock for trade, high case fatality among humans, and potential for human-to-human transmission [5].

* Corresponding author: Ahamed Mahdi Hassan

Ribavirin is the most studied antiviral drug for the treatment of CCHF, and it has been used both experimentally and in clinical settings. It works by inhibiting viral RNA synthesis and has shown promising results in vitro and vivo models. Some early observational clinical studies reported that ribavirin administered early in infection may reduce mortality. However, these studies were not randomised or controlled, which limits the strength of their conclusions [6]. However, other reports and systematic reviews found conflicting results, and a meta-analysis concluded that ribavirin did not significantly reduce overall mortality [7].

These efforts highlight the importance of repurposing known drugs as a faster, more cost-effective strategy than de novo drug development in response to emerging viral threats such as CCHF [8]. Several antiviral agents originally developed for other viral infections have been evaluated for their potential efficacy. For example, Ribavirin, initially used for hepatitis C and other RNA viruses, has been the most widely used drug in the management of CCHF. It demonstrated in vitro and vivo antiviral activity [6;7]. Nelfinavir is an antiviral drug used in the treatment of human immunodeficiency virus (HIV); it is a protease inhibitor that blocks the viral enzyme responsible for processing viral proteins, thereby preventing viral maturation and replication within the host [9].

Remdesivir, a nucleotide analogue originally developed for the Ebola virus, has since gained international use as a COVID-19 treatment due to its broad-spectrum antiviral pharmacological action [10]. Similarly, Sofosbuvir, an RNA-dependent RNA polymerase inhibitor approved for treating hepatitis C virus infection, has also been reported to have in silico-calculated antiviral activity against COVID-19 [11]. Darunavir (DRV) is an HIV-1 protease inhibitor indicated for use in combination with other antiretroviral agents for the treatment of HIV-1 infection in adults and pediatric patients three years of age and older [12].

It is a protease inhibitor that blocks HIV-1 protease activity, which is required for viral replication. Darunavir inhibits the host protease enzyme or viral maturation, thereby preventing particle maturation and increasing viral load, which slows viral spread in the body [13]. Favipiravir is an antiviral drug authorised in Japan for the treatment of influenza. It is an RNA-dependent RNA polymerase inhibitor [14]. Ritonavir is a type of antiretroviral medicine which treats human immunodeficiency virus (HIV) infection. It is classified as a protease inhibitor, although its main clinical use has shifted from a specific antiviral activity to a pharmacokinetic enhancer (booster) of other protease inhibitors [15]. This study aims to identify and priorities clinically licensed antiviral drugs that can be repurposed as inhibitors of CCHFV by implementing an in-silico workflow that couples high-throughput virtual screening, MD, and molecular dynamics refinement. Repurposing approved agents provides a rapid and cost-efficient path to therapeutics, an urgent need given CCHFV's case-fatality rate of up to 40 % and the current absence of licensed vaccines or antivirals.

2. Materials and Computational Methods

2.1 MD & MDS were conducted on a set of antiviral treatments selected for their potential effectiveness against CCHF. These compounds were chosen following an in silico evaluation suggesting their potential inhibitory activity against key viral proteins essential to the pathogenesis of CCHF. We obtained a three-dimensional structure of CCHF from the Protein Data Bank (PDB) using its corresponding PDB IDs.

2.1. Ligands Preparation

Six antiviral drugs were retrieved from the DrugBank database (Table 1). To perform the initial geometry optimization of their molecular structures, the semi-empirical AM1 method was employed using Hyper Chem version 8.08 to minimize their energy configurations [16,17]. Density Functional Theory (DFT) was employed to further refine the pre-optimized structures. The B3LYP functional with the 6-31G basis set was used to obtain the most stable conformations [18,19]. Gaussian 09 was used to calculate the global reactivity descriptors based on the optimized conformation [19,20]. The convergence criteria values are presented in Table 2 and were all satisfied ("YES") for maximum force, root-mean-square (RMS) force, maximum displacement, and RMS displacement. Additionally, the vibrational frequency calculations yielded only positive values, confirming that the optimized structures correspond to a true minimum on the potential energy surface and are not in a metastable state [21]. Optimized structures were then combined into a single database for the evaluation of ligand affinity with the MOE software.

Table 1 Antiviral agents selected for the study with their drug IDs.

Drugs	ID
Darunavir	DB01264
Favipiravir	DB12466
Nelfinavir	BD00220
Remdesivir	BD14761
Ritonavir	BD00503
Sofosbuvir	DB08934

2.1.1. Receptors Preparation

The 4AKL crystal structure of CCHF (Figure 1) was obtained from PDB (www.rcsb.org) using its specific ID [22]. Protein preparation was carried out using MOE software. In this process, polar hydrogen atoms were added, bond orders were assigned correctly, and the structure was refined for subsequent analysis. Missing side chains and loops, if any, were modelled automatically by the program. Water molecules located more than 3.0 Å away from heteroatoms were removed to eliminate irrelevant solvent interactions. The final structure was energy-minimized with MOE's default force field for optimal docking geometry. The active site was defined for ligand docking (Table 2).

Figure 1 Crystal structure of the CCHFV nucleocapsid (ID: 4AKL).

Table 2 The residues of the binding sites were utilized as input for receptor grid generation during the induced fit docking process.

Receptors	Residues
CCHF	3:(ALA57 ASP60 SER61 TYR63 ALA64 LEU67 VAL68 THR71 VAL152 MET173 ARG176 ARG177 ILE180 LEU181 SER295 ALA296 LEU297 ALA299 GLN300 ALA302 GLN303 ILE304 LEU334 GLY335 HIS337 PRO338 ARG339 GLY340 THR341 LYS342 MET344 ASP365 ARG372 ILE373 TYR374 MET375 THR381 ALA382 GLY383 ARG384 ILE385 SER386 GLU387 GLY408 HIS409 THR410 LYS411 MET446 ASP447 ILE448 VAL449 ALA450 GLU452 HIS453 LEU454 HIS456 GLN457 VAL460 ALA469 VAL472 LYS473 GLY474 ASN475 ALA476 THR477).

3. Results and Discussion

3.1. Molecular Docking

MD analysis performed on six antiviral compounds Ritonavir, Nelfinavir, Remdesivir, Darunavir, Sofosbuvir, and Favipiravir against the target protein CCHF. The results revealed variability in binding affinity (S-score) and molecular interactions, as summarized in Table 3.

Table 3 These results obtained from docking of antiviral agents.

Ligands	S score (Kcal/mol)	RMSD (Å)	Ligand atom	Receptor Atom	Receptor Residue	Interaction Type	Distance (Å)	E (Kcal/mol)
Darunavir	-6.9153	1.5055	O1 (4) O4 (16) C1 (1) N (36) 6-ring	OE1 O 6-ring OE1 NE	GLN 370 (A) VAL 117 (A) TYR 374 (A) GLU 116 (A) ARG 298 (A)	H-donor H-donor H-pi H-donor pi-cation	2.8 2.89 4.11 2.97 3.67	-0.9 -0.8 -0.5 -0.5 -0.9
Favipiravir	-3.8333	1.4996	O1 (4) O4 (16) C1 (1)	OE1 O 6-ring	GLN 370 (A) VAL 117 (A) TYR 374 (A)	H-donor H-donor H-pi	2.8 2.89 4.11	-0.9 -0.8 -0.5
Nelfinavir	-7.0805	1.4227	O1 (4) O4 (16) C1 (1) C (32) O (36)	OE1 O 6-ring O NH2	GLN 370 (A) VAL 117 (A) TYR 374 (A) VAL 117 (A) ARG 298 (A)	H-donor H-donor H-pi H-donor H-acceptor	2.8 2.89 4.11 3.25 3.05	-0.9 -0.8 -0.5 -0.5 -5.4
Remdesivir	-6.9161	1.5697	O1 (4) O4 (16) C1 (1) O (23) O (9) N (21) O (23)	OE1 O 6-ring OE1 NH2 CE NZ	GLN 370 (A) VAL 117 (A) TYR 374 (A) GLU 116 (A) ARG 298 (A) LYS 346 (B) LYS 346 (B)	H-donor H-donor H-pi H-donor H-acceptor H-acceptor H-acceptor	2.8 2.89 4.11 2.96 3.1 3.45 2.9	-0.9 -0.8 -0.5 -0.7 -2.6 -0.7 -3.1
Ritonavir	-7.1442	2.3697	O1 (4)	OE1	GLN 370 (A)	H-donor	2.8	-0.9

			O4 (16) C1 (1) O (23) O (9) N (21) O (23) O (36)	O 6-ring OE1 NH2 CE NZ NH2	VAL 117 (A) TYR 374 (A) GLU 116 (A) ARG 298 (A) LYS 346 (B) LYS 346 (B) ARG 298 (A)	H-donor H-pi H-donor H-acceptor H-acceptor H-acceptor H-acceptor	2.89 4.11 2.96 3.1 3.45 2.9 2.99	-0.8 -0.5 -0.7 -2.6 -0.7 -3.1 -2.6
Sofosbuvir	-6.4448	1.8384	O1 (4) O4 (16) C1 (1)	OE1 O 6-ring	GLN 370 (A) VAL 117 (A) TYR 374 (A)	H-donor H-donor H-pi	2.80 2.89 4.11	-0.9 -0.8 -0.5

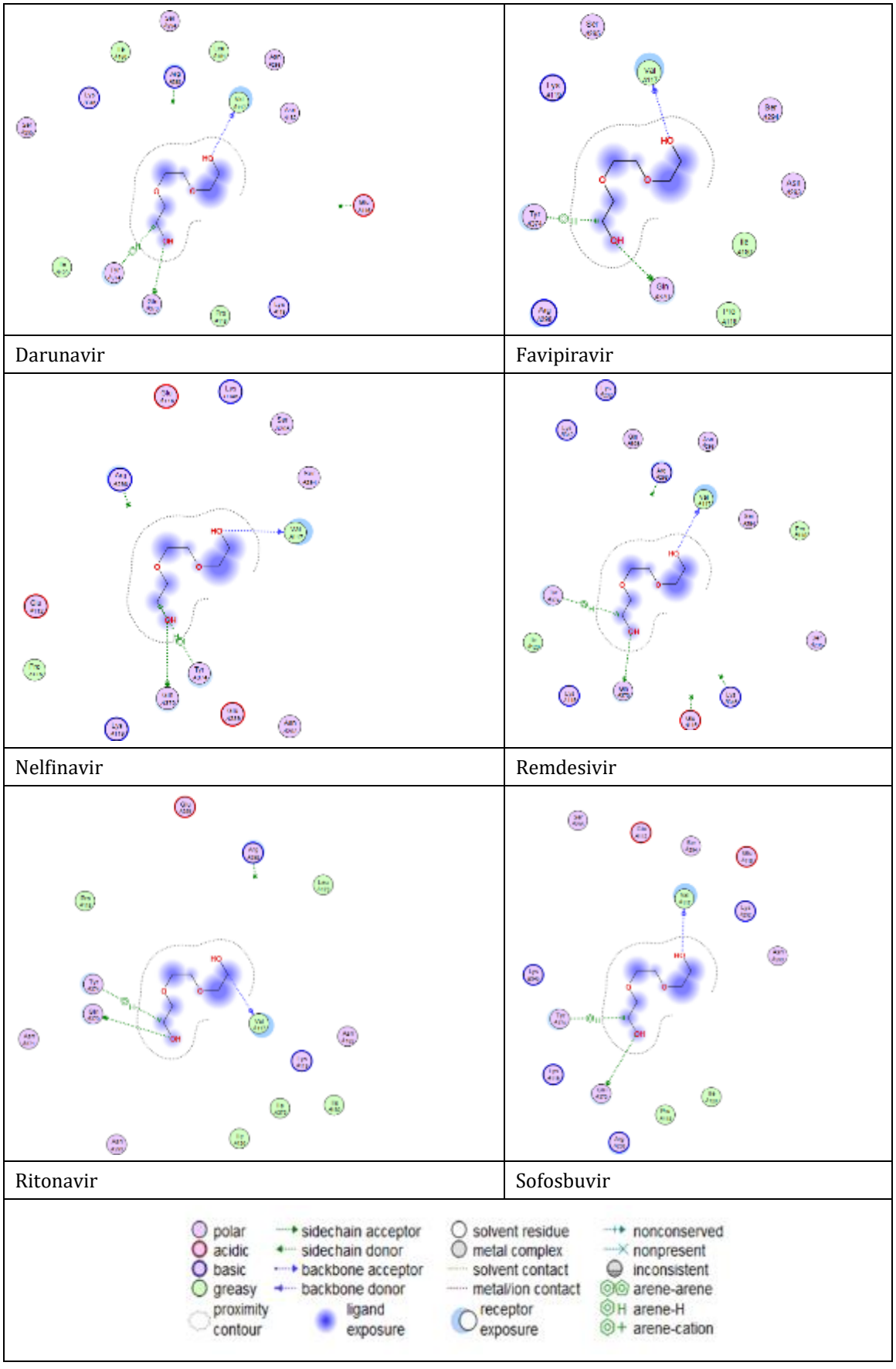

Figure 2 Interaction of the antiviral compound with the active site of 4AKL.

These findings suggest that Ritonavir and Nelfinavir possess the highest binding potential to the CH protein, making them promising candidates for further investigation as CH inhibitors.

3.2. Molecular Dynamics Simulation

Using Desmond 2020.1 [23]. MDS was carried out on the docked complexes of Nelfinavir, Remdesivir and Ritonavir.

The OPLS-2005 force field was used for simulations, and were solvated using an explicit solvent model, which added SPC water molecules to cubic periodic boundary conditions of 1.0 Å × 1.0 Å × 1.0 Å, and neutralized with sodium ions Na+ [24,25,26].

A simulated metabolic environment was created by the addition of a 0.15M NaCl solution [27]. First, the system was equilibrated by running the protein ligand complexes in an NVT ensemble for 10 ns. After NPT equilibration and minimization, a 12 ns NPT ensemble was used. The NPT ensemble was subjected to the Nose-Hoover chain coupling [28].

In simulations, only temperature was changed while the relaxation time (1.0 Ps) and pressure (1 bar) were fixed. We used a 2-femtosecond time step in all simulations. Pressure was regulated with the chain coupling barostat using a relaxation time of 2 ps [29].

Long-range electrical interactions were calculated according to the particle mesh Ewald method with the Coulomb interaction cutoff at 9 Å [30,31].

The equilibration of the bonded forces for each replica was carried out with the RESPA integrator with a time step of 2 fs. The ending production run was 100 ns per monomer.

Several important parameters such as root mean square deviation (RMSD), radius of gyration (Rg), root mean square fluctuation (RMSF), and hydrogen bond analysis (H-bonds) were employed to estimate the stability of MD simulations. These characteristics were employed to evaluate the global stability of the MDS. To assess the strength and stability of ligand-protein interactions, the binding free energy was determined using the Molecular Mechanics Generalized Born Surface Area (MM-GBSA) method. This analysis was performed on the MD simulation trajectories using the thermal_mmgbsa.py script, applying the VSGB solvation model along with the OPLS5 force field. Calculations were carried out over the last 10 frames of the trajectory, with a frame sampling interval of one.

The MM-GBSA approach estimates the binding affinity (ΔG_bind, in kcal/mol) based on the additive contributions of various energetic components. These components include electrostatic (Coulombic), van der Waals, hydrogen bonding, covalent, lipophilic interactions, self-contact corrections, and solvation energies of the ligand and protein.

The binding free energy (ΔG_bind) was computed using the following formula:

$$\Delta Gbind = \Delta GMM + \Delta GSolv - \Delta GSA$$

Where:

- ΔG_bind is the overall free energy of binding between the ligand and protein.
- ΔG_MM represents the difference in molecular mechanics energies between the complex and the sum of the separate protein and ligand energies.
- ΔG_Solv corresponds to the change in solvation energy upon complex formation, comparing the solvated complex with the solvated free ligand and receptor.
- ΔG_SA accounts for the change in surface area-dependent energy terms, reflecting non-polar contributions to solvation.

Figure 3 Also Shows the RMSD Profiles (ns) for Nelfinavir (Red), Remdesivir (Blue), and Ritonavir (Black) Ligand-Protein Complexes Over a 100 ns Molecular Dynamic Simulation Which Will Be Discussed Subsequently to Provide an Idea of Structural Stability and Dynamic Behavior of These Ligands. First, the RMSD values for all the complexes increase indicating for equilibration and a conformational adjustment in the binding pocket. The movement of nelfinavir

illustrates the gradual increase up to about 2.5 Å at 30 ns, after which there is only limited variation from the initial pose, indicative of convergence with only minor deviations, e.g., the peak of variance is at about 30 Å. The rapid rise of the RMSD of remdesivir to approximately 2.7 Å within 10 ns followed by a stable plateau with minor fluctuations is indicative of realistic conformational flexibility while showing an overall stable interaction with the protein. The RMSD value of ritonavir is a little higher than 3.0Å at some time pointsand also vibrates more frequently, indicating that it is more dynamic and reality. Although the interaction exhibits a significant RMSD peak as seen in coloration in (B) it indicates that the complex does not dissociate, nor does the complex show any other gross features of dissociation such as drastic coloration shown by a high RMSD of >22A (C). In general, the overall and the core RMSD values of all three complexes were in the range of acceptable limits which indicates stable nature of ligand-protein interaction. The equality of RMSD, as depicted by the steady RMSD profiles post- initial equilibration phase, indicates very good stability for each of the complex which indicates strong binding and less destabilization during the simulation. The comparative analysis indicates that Nelfinavir forms the most stable complex (migration RMSD (0.5), followed by Remdesivir (moderately stable complex migration RMSD 0.52), and Ritonavir which is more flexible but still retains overall integrity (migration RMSD 0.89; data not shown). These results indicate the binding behavior of each ligand was relatively stable and therefore potentially suitable for further development in structure-based drug design applications.

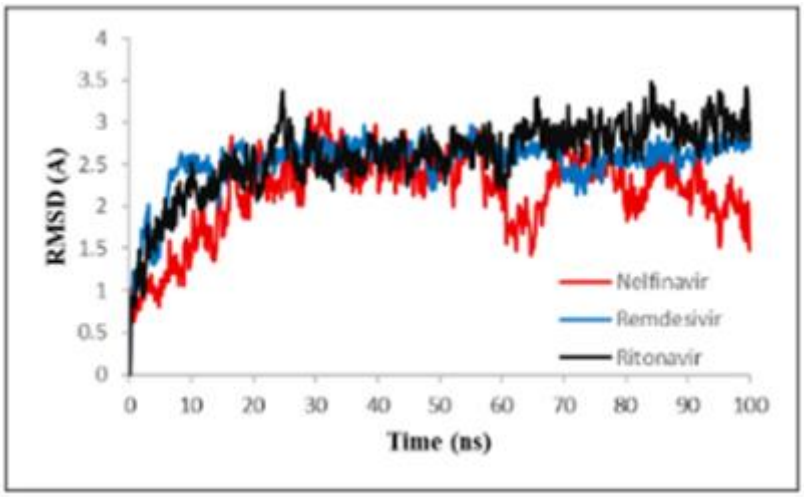

Figure 3 RMSD profiles three ligand-protein complexes over a 100 ns molecular dynamics simulation. The plot compares Nelfinavir (red), Remdesivir (blue), and Ritonavir (black), showing the structural deviation of each complex from its initial conformation.

The protein RMSF profiles highlighted in Figure 4 reflect the flexibility of single amino acid residues in the presence of three different ligands Nelfinavir (red), Remdesivir (blue), and Ritonavir (black) during the molecular dynamics simulation. In general, all three complexes are structurally rigid as most of the residues have RMSF in between 1–2 Å. On the other hand, certain regions in particular, among the 180 to 300 residue indices, showed higher RMSF values between 3–5 Å, indicating these regions are more flexible and may tend to be loop or surface-exposed regions. These malleable regions could be important for ligand recognition or allosteric regulation [3, 4]. Importantly, the peak for Ritonavir (black trace) displays the most prominent peak, just over 5 Å, indicating a region that has higher mobility that may correspond to areas of induced fit or spatial destabilization. By comparison, the Nelfinavir and Remdesivir red and blue traces exhibit only relatively modest fluctuations in the same area, suggesting a more conservative pattern of flexibility. Low RMSF values for all three ligands in the regions flanking both the N-terminal and C-terminal ends indicate stable secondary structure elements (e.g., helices or sheets). The specific segments of residue flexibility observed here may facilitate functional movements necessary for the accessibility of binding sites or provide flexibility needed for the catalytic activity. The corresponding lower peak RMSF values provide a better structural containment of dynamic motion than the complexed systems would bind better and may refer to gain in binding specificity or stability with the drug, a feature of the well-studied drugs like Nelfinavir and Remdesivir. Although all complexes exhibit specific characteristic movement at functional loops or binding interfaces, the characteristics and extents of these fluctuations differ subtly with each ligand and may alter the dynamic competence and functional output of the protein when interacting with ligand.

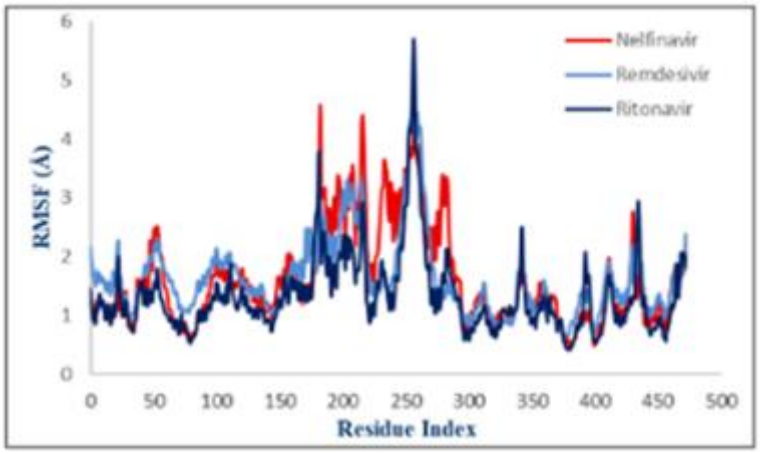

Figure 4 RMSF profiles of the protein residues bound to Nelfinavir (red), Remdesivir (blue), and Ritonavir (black) over the simulation period.

The Radius of Gyration (Rg) profiles depicted in Figure 5 highlight the overall compactness and folding behavior of the protein when bound to Nelfinavir (red), Remdesivir (blue), and Ritonavir (black) over a 100 ns molecular dynamics simulation. Each trace provides a measure of the mass-weighted root, which means square distance of atoms from the center of mass, reflecting how tightly the protein structure is folded. All three complexes begin with Rg values around 25.2 Å and gradually settle into more compact conformations. The complex with Remdesivir demonstrates the most consistent and lowest Rg values, typically fluctuating between 24.2 and 24.6 Å, indicating a tightly packed and stable folded state throughout the simulation. This suggests improved internal cohesion and potentially stronger interactions maintaining structural integrity. Ritonavir fluctuates a bit more, more markedly between 30 and 70 ns but is also almost entirely contained within 24.5–25.0 Å which indicates a gently compact state with putative relaxation events translating to slight structural changes at the binding site. Compared to the others in contrast, the Nelfinavir complex displays highest and most variable Rg values, showing a gradual upwards tendency towards the end of the simulation to above 25.0 Å, which could reflect a slight expansion or less compactness up to unfolding but not of the structural unfolding. Differences in Rg behavior across the three complexes reflect the effect of ligand binding on protein folding dynamics, where Remdesivir promotes the most compact and stable structure, consistent with an increased folding efficiency and structural stability.

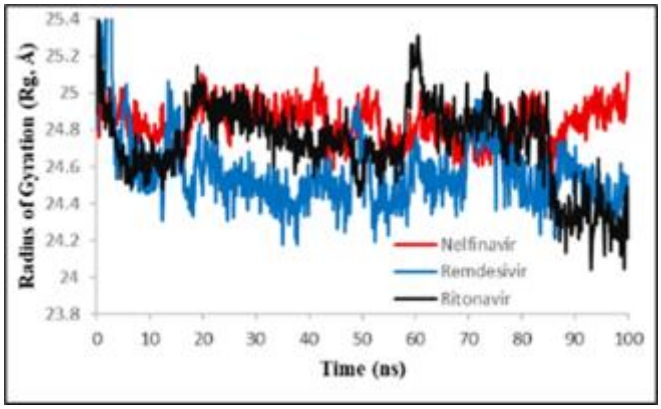

Figure 5 Radius of gyration (Rg) profiles of the protein bound to Nelfinavir (red), Remdesivir (blue), and Ritonavir (black) over 100 ns.

The relatively compact conformation adopted with substantial flexibility in the latter is supported as a collective; Ritonavir supports the N-termini with reasonable proximity to one another while Nelfinavir results in a somewhat more diffuse packing that cannot be more closely packed, possibly due to inefficient fit or weaker intermolecular contacts. In sum, The Rg analysis shows that all the ligand-bound states are folded and compact, although quite loosely (since these conformations are at least partially ordered, as their specific binding stabilizes folding in the exact conformation that was analyzed from the trajectory data).

The number of H-bonds formed is one of the most significant and stable interactions between protein and ligands which is presented in Figure 6, hints about the complex stability and binding affinity for the performed 100 ns molecular dynamics simulation. Red dashed lines indicate the number of H-bonds as a function of time between the drug and protein, and consistently throughout the simulation, Remdesivir (blue) shows the highest number of H-bonds ranging from 2–5 hydrogens, with several peaks up to 6 mostly in the second half of the simulation. That indicates a deep and stable interaction with the protein which probably explains the stability and compactness seen in the RMSD and Rg profiles of its respective complexes. Ritonavir (black) has a moderate hydrogen bonding profile, normally maintaining 1 to 3 H-bonds with occasional peaks of 4 to 5, consistent with a relatively stable interaction interspersed with periodic binding events. By comparison, Nelfinavir (red) establishes an overall lower number of H-bonds and never exceeding 2; in fact, after 50 ns hydrogen bonding drops to 0. The lower frequency of H-bonds means that the interaction with the protein is weaker and less stable, which would correspond to the previously higher Rg values and larger RMSD deviations seen in earlier analyses. Hydrogen bonds are important in orienting the ligand and stabilizing the complex, and their consistent formation throughout the simulation time is usually indicative of a strong fit of the ligand within the binding pocket. Thus, based upon the number and durability of H-bonds, the complex with Remdesivir has the most structurally stable interaction with the protein, whilst that with Ritonavir has a medium and stable interacting motif; that with Nelfinavir the least stable due to a lack of high occupancy and recurring contact points via hydrogen bonding. The differences reveal the influence of ligand orientation on competitive dynamics and may provide insight for additional design to enhance binding.

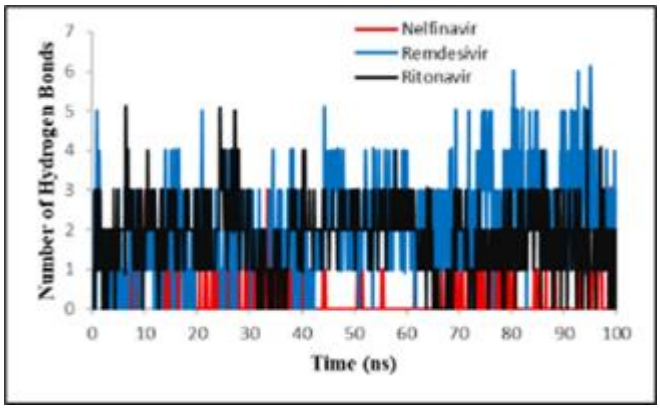

Figure 6 Number of H bonds formed between the ligands and protein over 100 ns. Remdesivir (blue) forms the highest and most consistent number of H-bonds, indicating strong and stable binding, followed by Ritonavir (black) with moderate stability, while Nelfinavir (red) shows the fewest bonds, suggesting weaker interactions.

The MM-GBSA binding free energy analysis revealed distinct energetic contributions influencing the interaction stability of Nelfinavir, Remdesivir, and Ritonavir with the target protein (Table 1). Among the three complexes, Remdesivir exhibited the most favorable binding affinity with a ΔGbind of –48.41 kcal/mol, closely followed by Nelfinavir (–47.76 kcal/mol), while Ritonavir demonstrated comparatively weaker binding with –27.37 kcal/mol. The van der Waals (ΔGbindvdW) interactions played a major stabilizing role, particularly for Remdesivir (–37.66 kcal/mol) and Ritonavir (–28.95 kcal/mol), indicating strong hydrophobic contacts, whereas Nelfinavir showed moderate vdW contribution (–20.12 kcal/mol). Lipophilic interactions (ΔGbindLipo) further enhanced binding, with Remdesivir again showing the highest contribution (–14.65 kcal/mol), suggesting significant nonpolar surface interactions. Electrostatic interactions (ΔGbindCoulomb) were consistently favorable across all complexes, notably in Nelfinavir (–14.51 kcal/mol), contributing to charge-based stabilization. Hydrogen bonding (ΔGbindHbond) made minor contributions in all cases, slightly more negative in Ritonavir (–1.35 kcal/mol), suggesting modest but specific polar interactions. The solvation penalty (ΔGbindSolvGB) was positive for all ligands, offsetting favorable terms to some extent, with the highest desolvation cost observed for Nelfinavir (22.14 kcal/mol), reflecting a greater energy requirement to desolvate polar surfaces. Covalent interaction energy (ΔGbindCovalent) and packing corrections (ΔGbindPacking) were relatively small contributors, with Remdesivir displaying the highest covalent interaction energy (2.60 kcal/mol), potentially indicating some strain upon binding. Overall, the strongest binding by Remdesivir appears to be driven by robust van der Waals and lipophilic interactions, whereas Nelfinavir benefited mainly from electrostatic and vdW forces. In contrast, the lower binding affinity of Ritonavir resulted from a combination of weaker vdW and lipophilic interactions and relatively high solvation cost, indicating reduced interaction stability within the binding pocket.

Table 4 MMGBSA analysis from binding energy calculations for Nelfinavir, Remdesivir and Ritonavir.

Energies (kcal/mol)	Nelfinavir	Remdesivir	Ritonavir
ΔG_{bind}	-47.76	-27.37	-48.41
$\Delta G_{bind}Lipo$	-6.15	-4.39	-14.65
$\Delta G_{bind}vdW$	-20.12	-28..95	-37.66
$\Delta G_{bind}Coulomb$	-14.51	-10.98	-10.07
$\Delta G_{bind}H_{bond}$	-0.64	-1.35	-0.71
$\Delta G_{bind}SolvGB$	22.14	18.82	19.10
$\Delta G_{bind}Covalent$	0.22	1.10	2.60
$\Delta G_{bind}Packing$	-0.69	-1.61	-1.23

The time series analysis of MDS for Nelfinavir reveals a consistent and stable binding mode within the protein's active site over a 100 ns trajectory (Figure7). At 0 ns, the ligand is well-positioned within the binding pocket, forming multiple van der Waals interactions along with H-bonds and π-alkyl interactions with key residues such as ASN182, GLU374, and ARG376. These interactions indicate a strong initial affinity and favorable orientation for binding. As the simulation progresses to 25 ns, the ligand undergoes a minor shift, still retaining crucial H-bonds and van der Waals interactions, particularly with ASN182, ARG376, and TYR374, suggesting a slight conformational adjustment to better fit the pocket. At 50 ns, the ligand becomes more embedded, maintaining hydrogen bonding with GLU374 and carbon hydrogen interactions with ARG376, while additional π-alkyl and alkyl interactions with residues like LEU374 and ALA302 support its stabilized orientation.

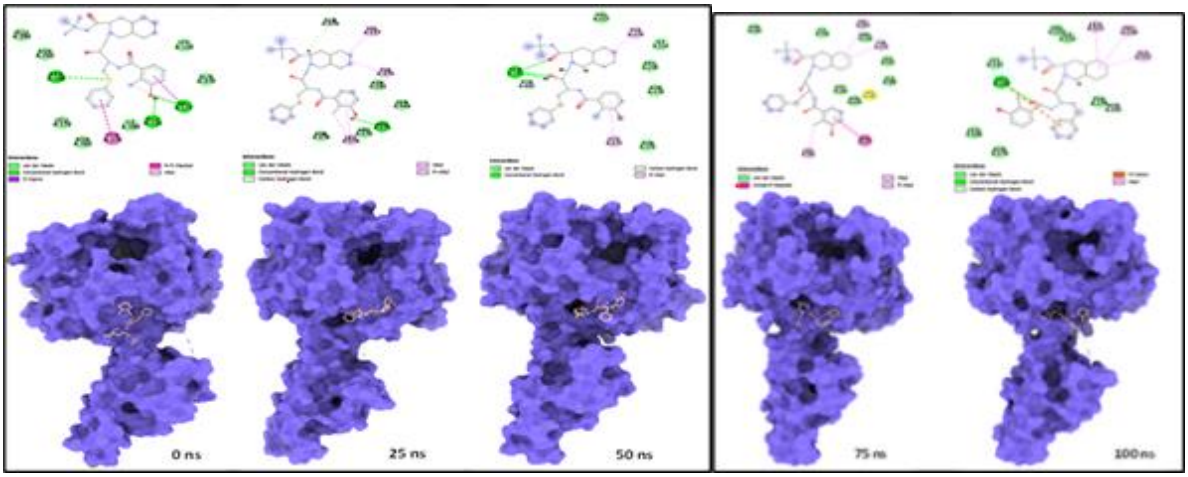

Figure 7 Time series analysis of Nelfinavir binding to the target protein over 100 ns MD simulation. Top panels show 2D interaction diagrams highlighting key residues and interaction types at different timepoints. Bottom panels display surface representations of the protein-ligand complex at 0, 25, 50, 75, and 100 ns, illustrating ligand stability and binding pocket occupancy throughout the simulation.

By 75 ns, the ligand displays strong π-alkyl and amide–π stacking interactions with residues such as TYR374, LEU374, and VAL117, while hydrogen bonding with ASN182 and ASN178 remains stable, indicating a tightly held and well-optimized binding conformation. At the final 100 ns mark, the ligand retains its deep position in the active site, reinforced by H-bonds with ARG298, ASN182, and TYR374, along with a new π-cation interaction involving ARG376, highlighting the evolving but increasingly stable interaction profile. Throughout the simulation, the surface representation shows that the ligand remains securely nestled within the binding pocket with minimal solvent exposure, and no signs of unbinding or major positional fluctuation are observed. The progressive strengthening of interactions and retention of core binding contacts over time reflect a favorable dynamic stability. This temporal consistency in the interaction network, including van der Waals, hydrogen bonds, π-interactions, and carbon hydrogen bonds, suggests a robust and energetically favorable ligand binding. Overall, the time-resolved structural insights

confirm Nelfinavir forms a highly stable and persistent complex with the protein throughout the 100 ns MDS, supporting its potential efficacy as a strong binder or inhibitor.

MDS (100ns) of the interaction of Remdesivir with the binding pocket of the target protein, have given an insight into the stability of the ligand within the pocket over the time series analysis (Figure8). At 0 ns, the ligand is similarly well-accommodated into the active site assisted mostly by the classical hydrogen bonding interactions with ASN178, ASN182, and ASN293 coupled with π-π T shaped interactions with TYR374 and VAL317. Initial binding is also aided through hydrophobic contacts such as π-alkyl and alkyl interactions with LEU179 and PRO118. When the simulation is extended to 25 ns, however, more subtle changes are apparent in ligand orientation: the ligand still forms H-bonds with ASN182 and ASN293, but changes in orientation allow it to also interact with ARG298 and GLN370, indicating flexibility and adaptability of the binding mode without substantial displacement. At 50 ns the ligand seems to rotate slightly, keeping essential hydrogen bonds and stabilizing contacts with LEU179 and ASN178 and also maintaining the hydrophobic contact with TYR374 and VAL317. At 75 ns, ligand is more stabilized in its binding pose as indicated by the strong hydrogen bond network with GLN370, ASN182 and ILE180. Moreover, π-π stacking interacts with TYR374 and hydrophobic contacts interact with LEU179 and VAL317, which preserved a dynamic but stable interaction profile. Lastly, at 100 ns, the position of the ligand is firmly lodged in the cavity with stable hydrogen bonding to ASN182, ASN293 and GLN370 and hydrophobic interaction with VAL317, ILE180 and TYR374 suggesting the ligand has reached a suitable thermodynamically favourable binding conformation. The ligand does not drift or is ejected during the course of the simulation, and the binding interactions are quite conserved throughout the course of the simulation, especially involving the key residue ASN182, ASN293, TYR374 and GLN370. A stable binding consists of hydrogen bonding, van der Waals forces as well as hydrophobic contact between the ligand and binding pocket, which confirms the affinity of ligand to the substrate pathway. These progressive snapshots illustrate the interplay between flexibility and stability, as small conformational adjustments enable the ligand to maximize its interactions, rendering the molecule with binding stability and modulator potential against the target protein throughout the simulation trajectory for Ritonavir.

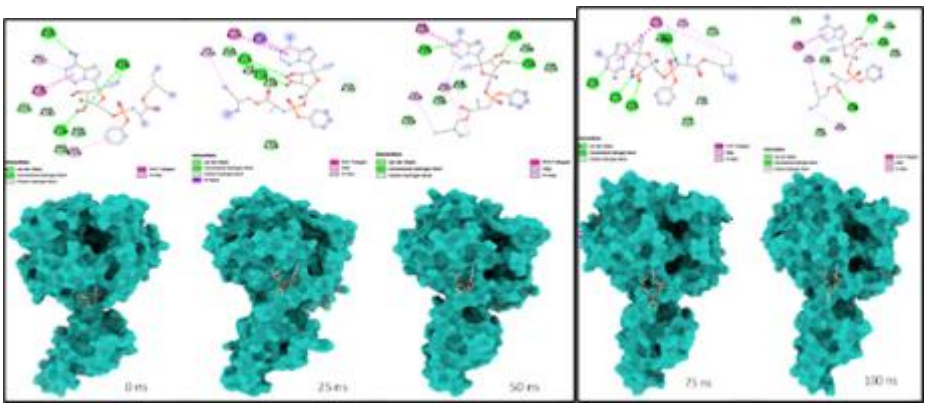

Figure 8 Time series analysis of Remdesivir within the protein binding pocket over a 100 ns molecular dynamics simulation. Top panels depict 2D interaction diagrams at 0, 25, 50, 75, and 100 ns, highlighting key hydrophobic, hydrogen bonds contacts, and π-interactions with surrounding residues. Bottom panels show corresponding 3D surface representations, illustrating the ligand's stable positioning and binding conformation throughout the simulation.

Time series analysis of Ritonavir over a 100 ns MD simulation shows dynamic yet stable binding behavior within the active site of the protein as seen from both 2D interaction diagrams and 3D surface representations (Figure 9). At 0 ns, the ligand filled the binding pocket forming conventional H-bonds with ASN293, ASN295, and LYS237, along with π-cation and π-anion interactions with ARG298 and TYR374, respectively. NCD also forms additional hydrophobic interactions with VAL290 and van der Waals contacts with multiple surrounding residues such as SER236, ALA250, which further stabilizes NCD. At 25 ns, the ligand has also moved by a few angstroms but still makes the critical interactions with ASN293, ARG298, and TYR374, moving into new π-alkyl and π-sulfur interactions with LEU179 and GLU294, consistent with a dynamic but stable binding profile. At 50 ns, the ligand continues to occupy similar orientation and key hydrogen bonds with ASN295 and LYS237, and π-interactions with TYR374 and ARG298 are further. In addition to this stability, there is deeper lodging in the hydrophobic pocket, manifested by persistent interactions with ALA250 and VAL290. At 75 ns, the ligand is profiled relatively buried in the binding pocket with tighter hydrogen bonding profile involving ASN293, ASN295, and SER236, persists with π-anion interaction with TYR374, while hydrophobic contact remains with VAL290 and LEU179 which indicates a strong binding with little position disentangle. The ligand is still tightly bound by 100 ns, with its core interaction profile preserved hydrogen bonds with

ASN293 and ASN295, π-cation contact with ARG298, and van der Waals and alkyl interactions with surrounding apolar residues (ALA250, LEU179, and TYR374). There are no indications of the ligand dissociating or diffusing from the binding site during the simulation, Receptor 3D surface views again consistently show the ligand buried within the cavity of the receptor. The retention of strong polar interactions, facilitated by an extensive π-system and non-polar contacts, highlights the structural complementarity and flexibility of the ligand with the active site. All together, these observations suggest that Ritonavir is able to attain a dynamically favorable and stable binding mode, with subtle conformational adjustments over time allowing for an optimization of its interaction landscape while remaining anchored within the binding pocket.

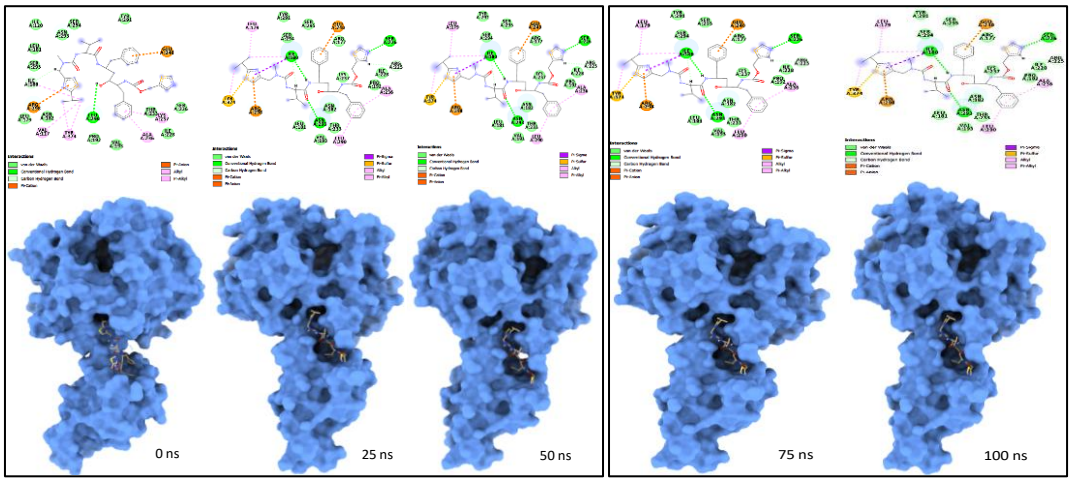

Figure 9 Time series analysis of Ritonavir within the protein binding pocket over a 100 ns molecular dynamics simulation. Top panels show 2D interaction diagrams at 0, 25, 50, 75, and 100 ns, highlighting hydrogen bonds, π-interactions, and hydrophobic contacts with key residues. Bottom panels display corresponding 3D surface representations, illustrating the ligand's stable binding orientation and consistent occupancy within the active site throughout the simulation.

4. Conclusion

In conclusion, the 100 ns MDS and MM-GBSA binding free energy analysis provided detailed insights into the dynamic stability and binding efficiency of Nelfinavir, Remdesivir, and Ritonavir within the target protein. Simulations were conducted using Desmond with the OPLS-2005 force field and SPC water model to replicate physiological conditions. Among the three, Nelfinavir showed the most consistent RMSD and stable binding profile, while Remdesivir exhibited the tightest packing and superior hydrogen bonding, indicating high structural integrity. Ritonavir displayed greater flexibility and RMSD variation, though it maintained structural cohesion. RMSF analysis highlighted flexible protein regions (residues 180–300), especially with Ritonavir. Rg values confirmed the compactness of all complexes, with Remdesivir being the most compact. MM-GBSA results identified Remdesivir as having the most favorable ΔG_bind (–48.41 kcal/mol), followed by Nelfinavir (–47.76 kcal/mol), both driven by strong van der Waals and electrostatic interactions. Ritonavir showed a weaker ΔG_bind (–27.37 kcal/mol) due to solvation penalties. Time-resolved interaction analysis confirmed stable hydrogen bonding and hydrophobic interactions for Nelfinavir (ASN182, ARG376, TYR374) and Ritonavir (ASN182, GLN370, TYR374). Overall, Remdesivir emerged as the most promising candidate due to its favorable binding energy, structural compactness, and stable interaction profile, highlighting the value of combined MD and MM-GBSA approaches in structure-based drug design.

Compliance with ethical standards

Acknowledgments

The author received no funding, institutional support or external help to carry out this work.

Disclosure of conflict of interest

The authors have no financial, personal or other relationships that could influence the work reported in this article

References

[1] Monsalve-Arteaga, L., Alonso-Sardon, M., Muñoz Bellido, J. L., Vicente Santiago, M. B., Vieira Lista, M. C., López Abán, J., ... & Belhassen-Garcia, M. (2020). Seroprevalence of Crimean-Congo hemorrhagic fever in humans in the World Health Organization European region: A systematic review. PLoS neglected tropical diseases, 14(3), e0008094. https://doi.org/10.1371/journal.pntd.0008094

[2] Ergönül, Ö. (2006). Crimean-Congo haemorrhagic fever. The Lancet infectious diseases, 6(4), 203-214. https://doi.org/10.1016/S1473-3099(06)70435-2

[3] Hawman, D. W., & Feldmann, H. (2023). Crimean–Congo haemorrhagic fever virus. Nature Reviews Microbiology, 21(7), 463-477. https://doi.org/10.1038/s41579-023-00871-9

[4] Ilboudo, A. K., Oloo, S. O., Sircely, J., Nijhof, A. M., & Bett, B. (2025). Spatial analysis and risk mapping of Crimean-Congo hemorrhagic fever (CCHF) in Sub-saharan Africa. Scientific Reports, 15(1), 2292. https://doi.org/10.1038/s41598-025-85873-8

[5] Mehand, M. S., Al-Shorbaji, F., Millett, P., & Murgue, B. (2018). The WHO R&D Blueprint: 2018 review of emerging infectious diseases requiring urgent research and development efforts. Antiviral research, 159, 63. https://doi.org/10.1016/j.antiviral.2018.09.009

[6] Fillâtre, P., Revest, M., & Tattevin, E. P. (2019). Crimean-Congo hemorrhagic fever: An update. Medecine et maladies infectieuses, 49(8), 574-585. https://doi.org/10.1016/j.medmal.2019.09.005

[7] Johnson, S., Henschke, N., Maayan, N., Mills, I., Buckley, B. S., Kakourou, A., & Marshall, R. (2018). Ribavirin for treating Crimean Congo haemorrhagic fever. Cochrane Database of Systematic Reviews, (6). https://doi.org/10.1002/14651858.CD012713.pub2

[8] Li, C., & He, W. Q. (2023). Global prediction of primary liver cancer incidences and mortality in 2040. Journal of Hepatology, 78(4), e144-e146. https://doi.org/10.1016/j.jhep.2022.12.002

[9] Muzammil, K., Rayyani, S., Abbas Sahib, A., Gholizadeh, O., Naji Sameer, H., Jwad Kazem, T., ... & Yasamineh, S. (2024). Recent advances in Crimean-Congo hemorrhagic fever virus detection, treatment, and vaccination: overview of current status and challenges. Biological Procedures Online, 26(1), 20. https://doi.org/10.1186/s12575-024-00244-3

[10] Dai, S., Deng, F., Wang, H., & Ning, Y. (2021). Crimean-Congo hemorrhagic fever virus: current advances and future prospects of antiviral strategies. Viruses, 13(7), 1195. https://doi.org/10.3390/v13071195

[11] Srivastava, S., Kumar, S., Sharma, P. K., Rustagi, S., Mohanty, A., Donovan, S., ... & Franco-Paredes, C. (2024). Control strategies for emerging infectious diseases: Crimean-Congo hemorrhagic fever management. Health Science Reports, 7(9), e70053. https://doi.org/10.1002/hsr2.70053

[12] Borrajo, A. (2025). Breaking barriers to an HIV-1 cure: innovations in gene editing, immune modulation, and reservoir eradication. Life, 15(2), 276. https://doi.org/10.3390/life15020276

[13] Spagnuolo, V., Castagna, A., & Lazzarin, A. (2018). Darunavir for the treatment of HIV infection. Expert Opinion on Pharmacotherapy, 19(10), 1149-1163. https://doi.org/10.1080/14656566.2018.1484901

[14] Matilla, F., Velleman, Y., Harrison, W., & Nevel, M. (2018). Animal influence on water, sanitation and hygiene measures for zoonosis control at the household level: A systematic literature review. PLoS neglected tropical diseases, 12(7), e0006619. https://doi.org/10.1371/journal.pntd.0006619

[15] Tsirizani, L., Waalewijn, H., Szubert, A., Mulenga, V., Chabala, C., Bwakura-Dangarembizi, M., ... & CHAPAS-4 trial team. (2025). Population pharmacokinetics of ritonavir as a booster of lopinavir, atazanavir, or darunavir in African children with HIV. Antimicrobial Agents and Chemotherapy, 69(11), e00771-25. https://doi.org/10.1128/aac.00771-25

[16] Jaramillo, P., Domingo, L. R., Chamorro, E., & Pérez, P. (2008). A further exploration of a nucleophilicity index based on the gas-phase ionization potentials. Journal of Molecular Structure: THEOCHEM, 865(1-3), 68-72. https://doi.org/10.1016/j.theochem.2008.06.022

[17] Stewart, J. J. (2013). Optimization of parameters for semiempirical methods VI: more modifications to the NDDO approximations and re-optimization of parameters. Journal of molecular modeling, 19(1), 1-32. https://doi.org/10.1007/s00894-012-1667-x

[18] Aljneed, F., Joudieh, N., Aljghami, I., Hussein, K., & Chamoun, N. (2025). Theoretical study of C36 and O@ C36 fullerene isomers with (C1, C2, Cs, D2, and D3h) symmetries: Geometry optimization, electrical properties, and spectroscopic analysis. AIP Advances, 15(6). https://doi.org/10.1063/5.0270996

[19] Nakata, M., & Maeda, T. (2023). PubChemQC B3LYP/6-31G*//PM6 data set: The electronic structures of 86 million molecules using B3LYP/6-31G* calculations. Journal of Chemical Information and Modeling, 63(18), 5734-5754. https://doi.org/10.1021/acs.jcim.3c00899

[20] Wahba, A. M., Shoueir, K., & Fouda, A. E. A. S. (2025). Prediction and evaluation of pyrimidinones derivatives: DFT analysis, corrosion inhibition, and bioactivity studies. Results in Surfaces and Interfaces, 18, 100448. https://doi.org/10.1016/j.rsurfi.2025.100448

[21] Niazi, S. K. (2025). Quantum mechanics in drug discovery: a comprehensive review of methods, applications, and future directions. International Journal of Molecular Sciences, 26(13), 6325. https://doi.org/10.3390/ijms26136325

[22] Carter, S. D., Surtees, R., Walter, C. T., Ariza, A., Bergeron, É., Nichol, S. T., ... & Barr, J. N. (2012). Structure, function, and evolution of the Crimean-Congo hemorrhagic fever virus nucleocapsid protein. Journal of virology, 86(20), 10914-10923. https://doi.org/10.1128/jvi.01555-12

[23] Bolcato, G., Bissaro, M., Pavan, M., Sturlese, M., & Moro, S. (2020). Targeting the coronavirus SARS-CoV-2: computational insights into the mechanism of action of the protease inhibitors lopinavir, ritonavir and nelfinavir. Scientific Reports, 10(1), 20927. https://doi.org/10.1038/s41598-020-77700-z

[24] Achappa, S., Aldabaan, N. A., Alasmary, M., Shaikh, I. A., Mahnashi, M. H., Desai, S. V., ... & Mannasaheb, B. A. (2025). Exploration of effective pharmacological inhibitors for NS5 protein through computational approach: A strategy to combat the neglected Kyasanur forest disease virus. Plos one, 20(7), e0325613. https://doi.org/10.1371/journal.pone.0325613

[25] Bouzina, A., Bouone, Y. O., Sekiou, O., Aissaoui, M., Ouk, T. S., Djemel, A., ... & Aouf, N. E. (2023). In vitro antitumor activity, molecular dynamics simulation, DFT study, ADME prediction, and Eg5 binding of enastron analogues. RSC advances, 13(28), 19567-19584. https://doi.org/10.1039/D3RA02904B

[26] Ali, R. H., Hussein, F. K., Nasar, D. M., & Abd Al salam Salem, A. (2025). The relevance of mitochondrial DNA mutation in human diseases and forensic sciences. Al-Nahrain Journal of Science, 28(1), 96-106. https://dx.doi.org/10.22401/ANJS.28.1.11

[27] Dehury, B., Mishra, S., Panda, S., Singh, M. K., Simha, N. L., & Pati, S. (2025). Structural Dynamics of Neutral Amino Acid Transporter SLC6A19 in Simple and Complex Lipid Bilayers. Journal of Cellular Biochemistry, 126(1), e30693. https://doi.org/10.1002/jcb.30693

[28] Vollmers, L., Chen, S.-Y., Reif, M., Mauck, T. A., & Zacharias, M. (2025). Molecular Dynamics: From Basics to Application [Article v1.0]. Living Journal of Computational Molecular Science, 6(1), 3797. https://doi.org/10.33011/livecoms.6.1.3797

[29] Sahil, M., Sarkar, S., & Mondal, J. (2023). Long-time-step molecular dynamics can retard simulation of protein-ligand recognition process. Biophysical Journal, 122(5), 802-816. https://doi.org/10.1016/j.bpj.2023.01.036

[30] Salman, H. A., Hussein, F. K., & Abdulrahman, S. J. (2024). A Comparison of Glutathione and Malondialdehyde Concentrations in Athletes Engaged in Certain Sports. Thamar University Journal of Natural & Applied Sciences, 9(1), 39-42. https://doi.org/10.59167/tujnas.v9i1.2053

[31] Pederson, J. P., & McDaniel, J. G. (2022). DFT-based QM/MM with particle-mesh Ewald for direct, long-range electrostatic embedding. The Journal of chemical physics, 156(17). https://doi.org/10.1063/5.0087386